Catalysis Today 157 (2010) 155–159

Contents lists available at ScienceDirect

Catalysis Today

journal homepage: www.elsevier.com/locate/cattod

Iron-modified ceria and Au/ceria catalysts for Total and Preferential Oxidation of CO (TOX and PROX)

O.H. Laguna [a,*], M.A. Centeno [a], G. Arzamendi [b], L.M. Gandía [b], F. Romero-Sarria [a], J.A. Odriozola [a]

[a] Departamento de Química Inorgánica e Instituto de Ciencia de Materiales de Sevilla Centro Mixto Universidad de Sevilla-CSIC, Avda. Américo Vespucio 49, 41092 Sevilla, Spain
[b] Departamento de Química Aplicada, Edificio de los Acebos, Universidad Pública de Navarra, Campus de Arrosadía, s/n, E-31006 Pamplona, Spain

ARTICLE INFO

Article history:
Available online 13 May 2010

Keywords:
Gold catalysts
Iron doped ceria
CO abatement
Preferential Oxidation (PROX)
Total Oxidation (TOX)

ABSTRACT

Iron-modified ceria supports containing different molar percentages of Fe (0%, 10%, 25%, and 50%) were synthesized by thermal decomposition of the metal propionates. The formation of a Ce–Fe oxide solid solution is evidenced through XRF, XRD, BET and Raman spectroscopy. For iron contents above 25% the formation of α-Fe_2O_3 was detected, pointing out the formation of the isolated oxides.

The catalytic activity of the Fe-modified catalysts in the Total Oxidation of CO reaction (TOX) is higher than for the bare CeO_2 material. The synergy between Ce and Fe shows a maximum for 10% Fe content (CeFe10), catalyst that shows the highest CO conversion per atom of Fe incorporated. Gold catalyst was also prepared on CeFe10 and its catalytic activity compared with Au/CeO_2 catalyst. The addition of iron to the gold catalyst resulted in an enhancement of the catalytic activity for CO oxidation especially at low temperature.

This Au/CeFe10 catalyst was also active and selective with excellent stability in the Preferential Oxidation of CO (PROX) showing a higher CO conversion than the Au/CeO_2 catalyst at temperatures below 150 °C being hardly affected by the presence of CO_2 and H_2O in the gas stream.

1. Introduction

The energy systems used nowadays are not sustainable. Because of it, energetic alternative models are necessary. The use of hydrogen as an energy vector represents one of these alternatives. H_2 is produced from fossil or renewable sources [1–3]. Removal of CO contamination from H_2-rich fuel gases is required for using hydrogen in polymer electrolyte fuel cells [4,5]. Therefore, the CO elimination reactions such us Total Oxidation (TOX) [3,6,7], Water Gas Shift (WGS) [8,9] and Preferential Oxidation (PROX) [10–12] are of relevance for the development of hydrogen based energetic infrastructure and has been thoroughly studied.

CeO_2 has been broadly reported as an active support for oxidation catalyst due to its structural properties [13,14]. This oxide has a redox behavior allowing high oxygen mobility, enhancing that way the oxygen exchange with the medium [15,16]. Additionally, it is well known that this oxygen mobility can be improved by the introduction of doping agents, with a different chemical nature, throughout the generation of a mixed system with a strong interaction, preferably as a solid solution in order to promote electronic distortions in the oxide framework [17,18]. Iron is an interesting candidate as a dopant, especially because it has its own redox behavior (Fe^{3+}/Fe^{2+}) [19–21].

On the other hand, gold supported catalysts are, in the CO conversion at low temperature, more active and selective than other noble metals [22,23]. However, the high activity of these systems strongly depends on the metallic dispersion and particle size of gold [24].

Therefore, taking into account the scenario presented above, the aim of this work is to study a series of CeO_2 supports doped with different proportions of Fe. The mixed oxide without phase segregation and the undoped ceria, for a comparative purpose, are selected for preparing 1% Au catalyst. Both systems are evaluated in the TOX and PROX reactions.

2. Experimental

2.1. Synthesis of the catalysts

A series of Ce–Fe mixed oxides (Fe content of 10, 25 and 50 mol%) were synthesized by a pseudo sol–gel method involving the thermal decomposition (500 °C, 2 h in air atmosphere) of the propionates. These mixed propionates were produced after dissolution of the adequate amounts of Ce(III) acetate and Fe(III)

* Corresponding author. Tel.: +34 954489501x9221; fax: +34 954460665.
E-mail addresses: oscarh@icmse.csic.es (O.H. Laguna), centeno@icmse.csic.es (M.A. Centeno), garzamendi@unavarra.es (G. Arzamendi), lgandia@unavarra.es (L.M. Gandía), francisca@icmse.csic.es (F. Romero-Sarria), odrio@us.es (J.A. Odriozola).

0920-5861/$ – see front matter © 2010 Elsevier B.V. All rights reserved.
doi:10.1016/j.cattod.2010.04.011

Table 1
Chemical analysis and cell parameter of the prepared solids.

Solid	Fe (mol%)	Cell parameter (Å)
Oxides		
CeO_2	–	5.405
CeFe10	9.5	5.386
CeFe25	24.7	5.383
CeFe50	49.3	5.402
Catalyst	**Au (wt.%)**	**Cell parameter (Å)**
Au catalysts		
Au/CeO_2	1.0	5.401
Au/CeFe10	0.9	5.383

acetyl acetonate in propionic acid (0.12 M) [25]. The nomenclature of the samples indicates the Fe content expressed as metallic mol% (CeFe10, CeFe25 and CeFe50). Pure CeO_2 support was synthesized by the same method in order to compare with the mixed systems.

Gold catalyst (1 wt.%) was prepared by the deposition–precipitation method over the selected supports (CeFe10 and CeO_2), at 70 °C and pH = 8 using chloroauric acid as gold source. The obtained solids (Au/CeFe10 and Au/CeO_2) were washed with deionized water until total chloride removal, dried overnight at 60 °C and finally, calcined 2 h at 300 °C.

2.2. Characterization

X-ray fluorescence (XRF) spectrometry was carried out in an X Panalytical AXIOS PW4400 with Rh tube. Powder X-ray diffraction (XRD) patterns were recorded on a Siemens D500, using Cu Kα radiation, 0.05° step size and 1 s step time. Raman spectra were recorded in a dispersive Horiva Jobin Yvon LabRam HR800 Confocal Raman Microscope (green laser 532.14 nm, 2 mW).

2.3. Catalytic activity

For the TOX reaction, the catalysts were pretreated in a 30 mL/min activation flow of 21% O_2 balanced in He. The light-off curves (from room temperature to 300 °C, 5 °C/min) were obtained with a 42 mL/min reactive stream of 3.4% CO and 21% O_2 in He. The reaction was carried out in a conventional continuous flow U-shaped glass reactor working at atmospheric pressure where 80 mg of sample was placed between glass wools. The reaction was followed by mass spectrometry (Balzers® Thermostar).

PROX reaction was carried out at atmospheric pressure on a cylindrical fixed bed reactor of stainless steel (9 mm inner diameter), with 100 mL/min of a reaction feed composed by 2% CO, 1% O_2, 50% H_2 and N_2 as balance. To study the effect of H_2O and CO_2, 10% of both compounds were added to the feed. The catalyst (100 mg, particle size in the 100–200 μm range) was diluted with crushed glass particles in the same particle size range forming a bed of about 5 mm in length. Products and reactants were separated and quantified by on-line gas chromatography (Agilent® 7890) equipped with a Porapak® Q, two Mole Sieve 5A, and two Hayesep® Q columns and a TCD detector.

Prior to the catalytic measurements, the samples were treated under a 15 mL/min flow of 21% O_2 in N_2, at 300 °C for 1 h.

3. Results and discussion

3.1. Oxides

The XRF results presented in Table 1 show that all the doped solids have iron contents close to the nominal values. Similar results have been reported for mixed oxides synthesized by the same method [25,26], indicating that the thermal decomposition of the propionates promotes the interaction of the cations enhancing the homogeneity of the obtained solid [26].

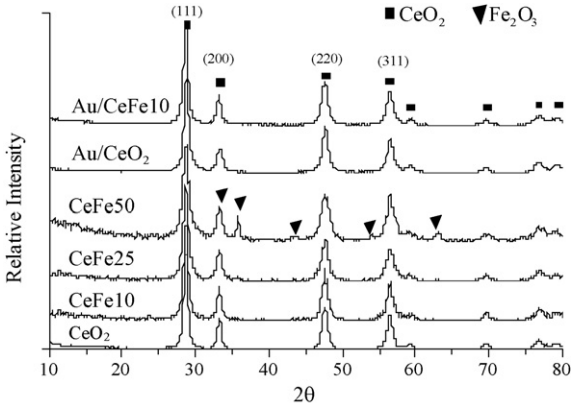

Fig. 1. XRD pattern of the prepared solids.

The XRD analysis of CeO_2 and the Fe-doped solids are presented in Fig. 1. In all the cases, the patterns correspond to the c-CeO_2 fluorite structure (JCPDS 00-034-0394). However, for the oxides with the higher Fe content (25% and 50%), additional signals assigned to hematite-like iron oxide (α-Fe_2O_3 JCPDS 00-033-664) can be seen.

The cell parameter values of the solids, calculated from the (1 1 1), (2 0 0), (2 2 0), and (3 1 1) reflections are included in Table 1. The bare CeO_2 solid and the material with the higher iron content have similar cell parameters. Nevertheless, for Fe contents up to 25% the cell parameter decreases as the iron content. This suggests the formation of a solid solution, since it has been reported that the introduction of iron in the CeO_2 fluorite structure results in a contraction of the unit cell due to the smaller ionic radii of iron compared to that of cerium [19–21,27]. The coincidence in cell parameters of CeO_2 and CeFe50 catalysts is consistent with the presence of α-Fe_2O_3 in the solids with the higher iron content, pointing out the existence of a solubility limit of iron in the ceria matrix. In our case, the 25% iron content is close to the solubility limit reported by Bao et al. (30%) [19].

Fig. 2 shows the Raman spectra of the studied oxides. Pure CeO_2 presents two main bands. The most intense one at 461 cm^{-1} is ascribed to the Raman active F_{2g} mode and corresponds to the oxygen symmetric breathing vibration around Ce^{4+} [15]. The very weak band at 598 cm^{-1} is assigned to the presence of oxygen vacancies

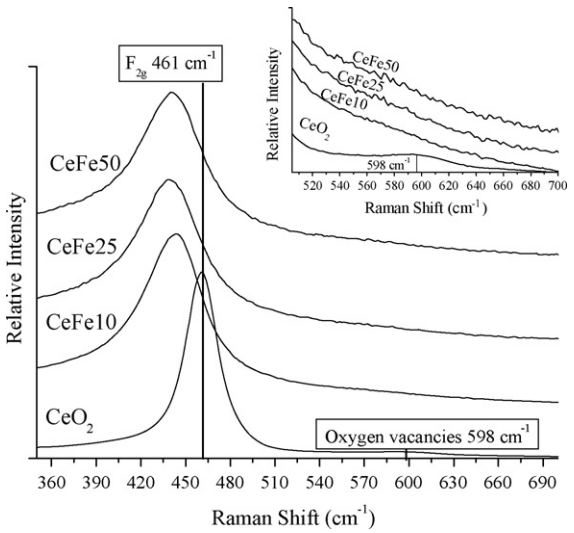

Fig. 2. Raman spectra of the oxides.

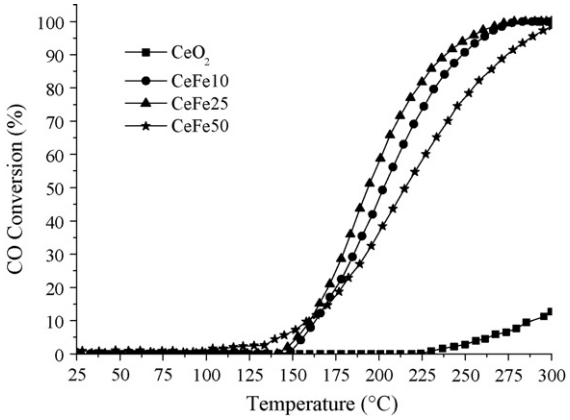

Fig. 3. Light-off curves of the prepared oxides in the TOX reaction ($T50_{TOX}$ values: CeO_2 = >300 °C; CeFe10 = 203 °C; CeFe25 = 193 °C; CeFe50 = 215 °C).

in the structure [28] and is indicative of the existence of Ce^{3+} ions [15,28,29].

For the iron doped samples, the F_{2g} band shifts towards lower frequencies and becomes broader on increasing the iron content probably due to the Ce–Fe interaction. The decrease in the particle size and/or the modification of the lattice symmetry in the case of formation of solid solution may account for this behavior [15,19–21]. On the other hand, the band due to oxygen vacancies disappears for the doped systems (Fig. 2, inset). Some authors associated this behavior to the interaction of Fe^{3+} ions placed at interstitial positions of the fluorite structure with the oxygen vacancies [19,27]. The Raman spectroscopy evidences the existence of a Ce–Fe interaction in all the studied doped samples, even if hematite phase segregation occurs.

The light-off curves of the oxides in the TOX reaction are presented in Fig. 3 and the respective temperature values for a CO conversion of 50% ($T50_{TOX}$) are showed in the figure caption. It is observed that Fe-modified solids show higher CO conversion than pure CeO_2. Among the Fe-modified solids the conversion is higher when the solid solution is favored.

The CeFe50 solid shows smaller CO conversion than the iron–cerium solid solution since phase segregation decreases the Ce–Fe interaction. It has been reported that the reducibility of Ce and Fe is enhanced when a close contact between both cations is possible resulting in higher stability of the reducible species if they are forming a solid solution [19,21]. The enhanced reducibility of the support increases the concentration of sites in the structure with a high electronic density and promotes the activation of the CO molecule on the surface during the TOX reaction. In Fig. 4 the

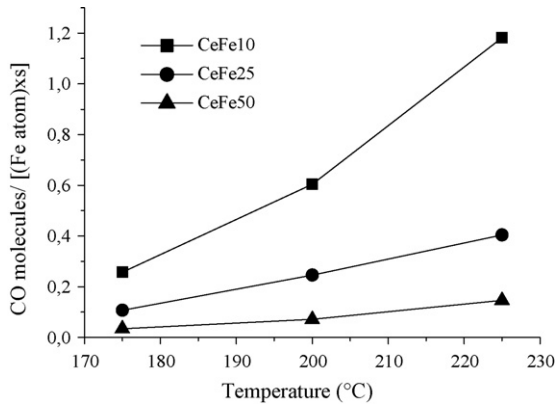

Fig. 4. CO oxidation rate per atom in the oxide (TOX reaction).

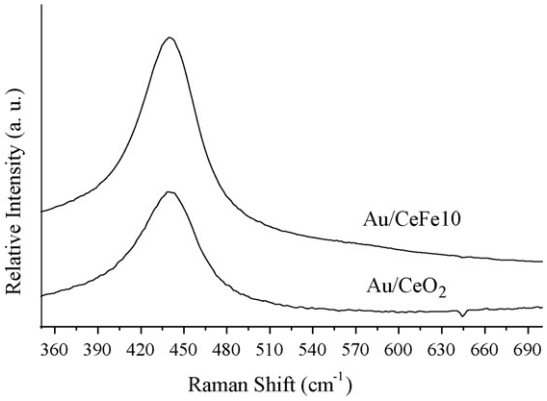

Fig. 5. Raman spectra of the prepared gold catalysts.

number of CO molecules converted per iron atom per second is shown by all the studied supports. The lower the iron content in the solid, the higher the amount of CO molecules converted [19].

These results indicate that the support, in which only a Ce–Fe solid solution is detected, has the highest efficiency in the CO conversion per iron atom. Therefore, taking into account the high homogeneity, the highest efficient interaction and the highest CO conversion per iron site, the support CeFe10 is selected for depositing gold.

3.2. Gold catalysts

XRF analysis (Table 1) shows that Au/CeO_2 and Au/CeFe10 have gold loadings which correspond with the target value (1%). On the other hand, the absence signals in the XRD pattern that may be assigned to metallic gold is indicative of the small size of the gold particles (typically less than 4 nm) [22,24,30].

The Raman spectra of the gold catalysts are presented in Fig. 5. The addition of gold does alter neither the lattice parameters obtained by XRD (Table 1) nor the frequency of the F_{2g} vibrational mode. The Raman band associated to the presence of oxygen vacancies in the ceria lattice disappears in the Au/CeO_2 catalyst with respect to pure ceria and remains absent in both Au/CeFe10 and CeFe10 materials. These results indicate that oxygen vacancies are preferential sites for gold anchoring on the support surface. The role of the CeO_2 oxygen vacancies, as a promoter of the gold dispersion, has been previously reported [31]. In the case of Au/CeFe10, the mechanism of gold deposition promotes a high dispersion according to XRD analyses; however complementary studies are required in order to explain the formation of small gold particles without the presence of oxygen vacancies.

In Fig. 6, the catalytic activity of the gold catalysts is compared with that of their corresponding supports and the respective temperature values for a CO conversion of 50% ($T50_{TOX}$) are presented in the figure caption. It is evident that the promoting effect of Au, because in both systems, a 100% CO conversion is obtained at temperatures below 100 °C. Nevertheless, the Au/CeFe10 solid has a better behavior than Au/CeO_2 one in the TOX reaction.

The studied catalysts and their respective supports were also tested in the PROX reaction (Fig. 7). The temperature values for a CO conversion of 50% ($T50_{PROX}$) are presented in the figure caption. The promoting effect of the Ce–Fe interaction increases the CO conversion of the support with respect to pure ceria, although the highest difference is observed when gold is added to the catalyst. The difference between Au/CeO_2 and Au/CeFe10 is more evident in the PROX reaction than in the TOX one, especially at temperatures below 140 °C. The CO conversion over Au/CeFe10 is closer to the equilibrium one (Fig. 7), probably due to the reducing character of

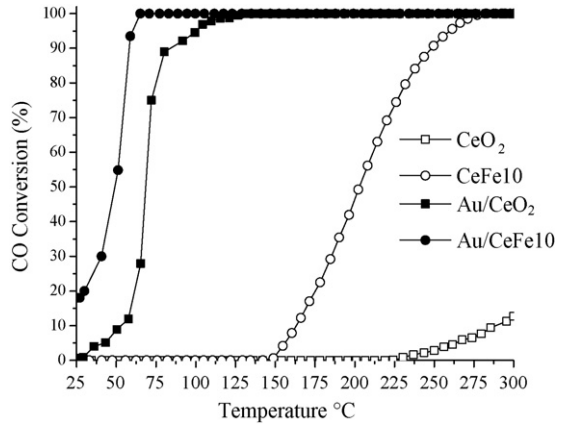

Fig. 6. CO conversion in the TOX reaction over the gold catalysts and the corresponding supports ($T50_{TOX}$ values: CeO_2 = >300 °C; CeFe10 = 203 °C; Au/CeO_2 = 69 °C; Au/CeFe10 = 49 °C).

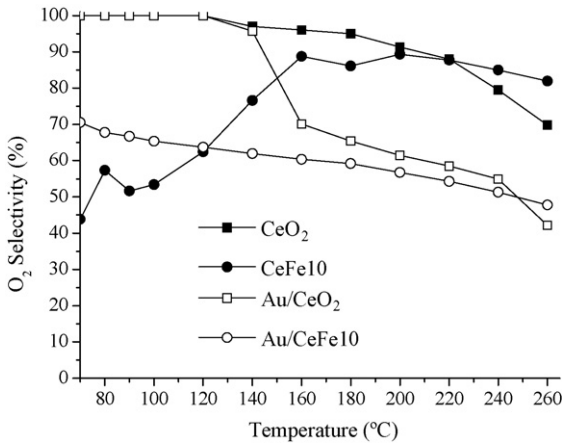

Fig. 8. Selectivity to CO conversion in the PROX reaction for the prepared gold catalysts.

the H_2-rich reaction. In this case, the reducing atmosphere favors the stability of the Ce and Fe reduced species, the high electronic density of these reduced species promotes the CO activation on the catalyst surface. Additionally the synergy between the mixed support and Au enhances the reducibility and the oxygen exchange of the solids, being the reason of the high activity of the Au/CeFe10 catalyst.

Fig. 8 shows the selectivity to CO oxidation in the PROX reaction presented by the gold catalysts and their respective supports. In the case of the supports, pure ceria has the highest selectivity close to 100% in the studied temperatures, but its poor catalytic activity must be considered. The CeFe10 support presents a lower selectivity, although it increases with temperature reaching 90% at temperatures higher than 160 °C. The Au/CeFe10 solid is less selective for CO oxidation than the Au/CeO_2 catalyst below 140 °C although it must be pointed out that Au/CeFe10 is significantly more active under these conditions.

In order to perform a more appropriate comparison of the catalyst selectivities, temperatures have been restricted to the 180–240 °C range in Fig. 9 because under these conditions the CO conversions in the PROX reaction provided by the two gold catalysts is similar. As can be seen, the superior selectivity of Au/CeO_2 is confirmed. As the CO conversion is very similar over both catalysts, this implies that the rate of H_2 oxidation is higher over Au/CeFe10. This behavior could be related to the interaction between Au, Fe and Ce giving rise to the creation of new or more active sites for the activation of H_2 over Au/CeFe10. Additionally the H_2O formation is thermodynamically favored if temperature is increased (Fig. 7).

Deviation from equilibrium conditions is due to parallel processes such as the Water Gas Shift (WGS) or even the Reverse Water Gas Shift (RWGS) reactions. Therefore, some authors have studied the modification mechanism of activation of CO molecules in the presence of H_2O and CO_2 [32,33]. From previously published data it can be inferred that there is competitive adsorption between CO and the other species, during the reactants adsorption step. This behavior depends on the composition of the PROX reaction feed stream and temperature, among other variables [34]. Taking into account that the PROX reaction feed usually comes from reforming and WGS reactors, the effect of the presence of CO_2 and H_2O (below 30%) in the reaction mixture must be considered. Some authors have reported on the influence of CO_2 and H_2O in the PROX reaction [32]. In our work, the most active catalyst (Au/CeFe10) was selected for evaluation under a PROX feed with 10% CO_2 and 10% H_2O. In Fig. 10 the results obtained in the presence and absence of water and CO_2 in the feed are compared.

The CO conversion in the PROX reaction is hardly modified when H_2O and CO_2 are added to the reaction mixture. This suggests that the active sites remain almost unaffected under excess of H_2O and CO_2. The high activity exhibited by the catalyst at temperatures around 100 °C is an interesting result because this temperature is close to the operating conditions of low-temperature fuel cells.

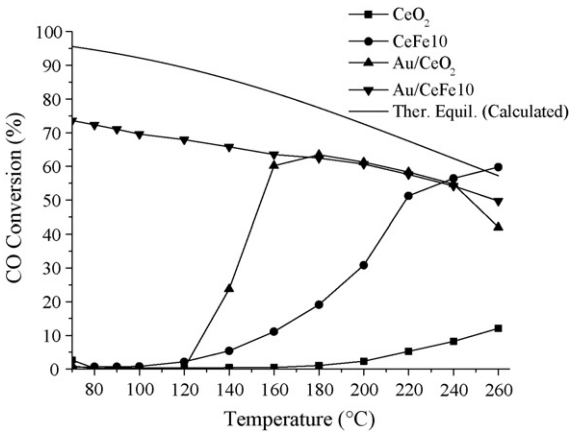

Fig. 7. CO conversion in the PROX reaction over the gold catalysts and the corresponding supports ($T50_{PROX}$ values: CeO_2 = >300 °C; CeFe10 = 218 °C; Au/CeO_2 = 155 °C; Au/CeFe10 = <70 °C).

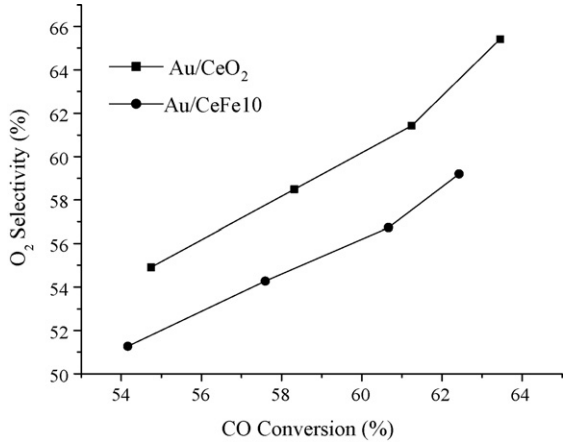

Fig. 9. Selectivity to CO conversion in the PROX reaction for the prepared gold catalysts in the 180–240 °C temperature range.

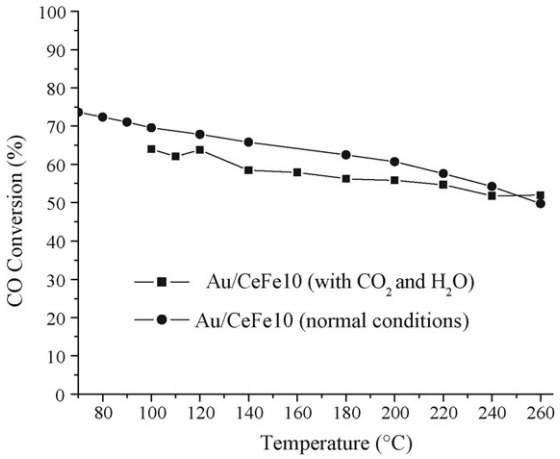

Fig. 10. CO conversion in the PROX reaction over the Au/CeFe10 catalyst in the presence and absence (normal conditions) of H_2O and CO_2.

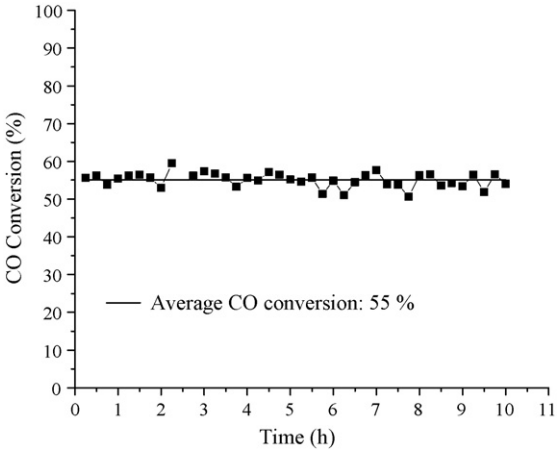

Fig. 11. Catalytic stability in PROX reaction of Au/CeFe10 catalyst at 160 °C, with H_2O and CO_2 in the feed.

The stability of the Au/CeFe10 catalyst at an intermediate temperature (160 °C) with H_2O and CO_2 in the feed was also investigated, and the results are presented in Fig. 11.

No loss of activity is evidenced for at least 10 h, which is a promising result for the potential application of this catalyst for the cleaning of H_2 for use in fuel cells.

4. Conclusions

The introduction of Fe into the CeO_2 network results in Ce–Fe interaction through the formation of a solid solution. This behavior is particularly effective for the lowest iron content (10%), where no iron oxide segregation is detected.

A gold catalyst prepared with the CeFe10 as support is a very active for both, TOX and PROX reactions, especially at low temperatures compared with Au/CeO_2.

The Au/CeFe10 catalyst maintains its catalytic performances in the presence of H_2O and CO_2 in the reactor feed. In addition, the catalyst is stable at 160 °C, at least, for 10 h.

Acknowledgements

O.H. Laguna thanks Ministerio de Ciencia e Innovación de España/Programa FPI for his financial support by the scholarship MCYT (MAT2006-12386-C05). F. Romero-Sarria also thanks the Ministerio de Ciencia e Innovación for her Ramon y Cajal contract.

References

[1] G. Arzamendi, P.M. Diéguez, M. Montes, M.A. Centeno, J.A. Odriozola, L.M. Gandía, Catal. Today 143 (2009) 25.
[2] G. Arzamendi, P.M. Diéguez, M. Montes, J.A. Odriozola, E. Falabella Sousa-Aguiar, L.M. Gandía, Chem. Eng. J. 154 (2009) 168–173.
[3] F. Romero-Sarria, A. Penkova, L.M. Martinez, T.M.A. Centeno, K. Hadjiivanov, J.A. Odriozola, Appl. Catal. B 84 (2008) 119.
[4] P. Biswas, D. Kunzru, Int. J. Hydrogen Energy 32 (2007) 969.
[5] H. Chen, T. Zhang, B. Dou, V. Dupont, P. Williams, M. Ghadiri, Y. Ding, Int. J. Hydrogen Energy 34 (2009) 7208.
[6] L.M. Martínez, T.D.M. Frías, M.A. Centeno, A. Paúl, M. Montes, J.A. Odriozola, Chem. Eng. J. 136 (2008) 390.
[7] J.G. Carriazo, L.M. Martínez, J.A. Odriozola, S. Moreno, R. Molina, M.A. Centeno, Appl. Catal. B 72 (2007) 157.
[8] M. Boaro, M. Vicario, J. Llorca, C. de Leitenburg, G. Dolcetti, A. Trovarelli, Appl. Catal. B 88 (2009) 272.
[9] X. Du, D. Gao, Z. Yuan, N. Liu, C. Zhang, S. Wang, Int. J. Hydrogen Energy 33 (2008) 3710.
[10] G. Avgouropoulos, J. Papavasiliou, T. Ioannides, Catal. Commun. 9 (2008) 1656.
[11] G. Avgouropoulos, J. Papavasiliou, T. Tabakova, V. Idakiev, T. Ioannides, Chem. Eng. J. 124 (2006) 41.
[12] M. Manzoli, G. Avgouropoulos, T. Tabakova, J. Papavasiliou, T. Ioannides, F. Boccuzzi, Catal. Today 138 (2008) 239.
[13] C. Mondelli, V.D. Santo, A. Trovarelli, M. Boaro, A. Fusi, R. Psaro, S. Recchia, Catal. Today 113 (2006) 81.
[14] A. Trovarelli, C. de Leitenburg, M. Boaro, G. Dolcetti, Catal. Today 50 (1999) 353.
[15] W.Y. Hernández, M.A. Centeno, F. Romero-Sarria, J.A. Odriozola, J. Phys. Chem. C 113 (2009) 5629.
[16] G. Avgouropoulos, M. Manzoli, F. Boccuzzi, T. Tabakova, J. Papavasiliou, T. Ioannides, V. Idakiev, J. Catal. 256 (2008) 237.
[17] X. Song, N. Jiang, Y. Li, D. Xu, G. Qiu, J. Rare Earth 25 (2007) 428.
[18] L. Ilieva, G. Pantaleo, I. Ivanov, R. Zanella, A.M. Venezia, D. Andreeva, Int. J. Hydrogen Energy 34 (2009) 6505.
[19] H. Bao, X. Chen, J. Fang, Z. Jiang, W. Huang, Catal. Lett. 125 (2008) 160.
[20] F.J. Pérez-Alonso, M.L. Granados, M. Ojeda, T. Herranz, S. Rojas, P. Terreros, J.L.G. Fierro, M. Gracia, J.R. Gancedo, J. Phys. Chem. B 110 (2006) 23870.
[21] F.J. Pérez-Alonso, T. Herranz, S. Rojas, M. Ojeda, M. López Granados, P. Terreros, J.L.G. Fierro, M. Gracia, J.R. Gancedo, Green Chem. 9 (2007) 663.
[22] M. Haruta, Catal. Today 36 (1997) 153.
[23] G. Panzera, V. Modafferi, S. Candamano, A. Donato, F. Frusteri, P.L. Antonucci, J. Power Sources 135 (2004) 177.
[24] M.Á. Centeno, C. Portales, I. Carrizosa, J.A. Odriozola, Catal. Lett. 102 (2005) 289.
[25] H. Provendier, C. Petit, J.L. Schmitt, A. Kiennemann, C. Chaumont, J. Mater. Sci. 34 (1999) 4121.
[26] F. Romero-Sarria, J.C. Vargas, A.-C. Roger, A. Kiennemann, Catal. Today 133–135 (2008) 149.
[27] F.J. Pérez-Alonso, M. Ojeda, T. Herranz, S. Rojas, J.M. González-Carballo, P. Terreros, J.L.G. Fierro, Catal. Commun. 9 (2008) 1945.
[28] J.E. Spanier, R.D. Robinson, F. Zhang, S.W. Chan, I.P. Herman, Phys. Rev. B: Condens. Mater. Phys. 64 (2001) 2454071.
[29] V.G. Keramidas, W.B. White, J. Chem. Phys. 59 (1973) 1561.
[30] M.I. Domínguez, F. Romero-Sarria, M.A. Centeno, J.A. Odriozola, Appl. Catal. B 87 (2009) 245.
[31] K. Qian, S. Lv, X. Xiao, H. Sun, J. Lu, M. Luo, W. Huang, J. Mol. Catal. A: Chem. 306 (2009) 40.
[32] H.C. Lee, D.H. Kim, Catal. Today 132 (2008) 109.
[33] E. Moretti, L. Storaro, A. Talon, P. Patrono, F. Pinzari, T. Montanari, G. Ramis, M. Lenarda, Appl. Catal. A 344 (2008) 165.
[34] D. Gamarra, A. Martínez-Arias, J. Catal. 263 (2009) 189.